JOURNAL OF GEOPHYSICAL RESEARCH, VOL. 94, NO. C2, PAGES 2005–2021, FEBRUARY 15, 1989

Mixing in the Equatorial Surface Layer and Thermocline

JAMES N. MOUM, DOUGLAS R. CALDWELL, AND CLAYTON A. PAULSON

College of Oceanography, Oregon State University, Corvallis

Twelve days of microstructure measurements at the equator (140°W) in November 1984 showed a surprisingly strong effect of both the daily cycle of solar heating and wind on mixing in the upper ocean. Because of limited variations in atmospheric forcing and currents during the experiment, processes in the daily mixing cycle were similar from day to day. Only the intensity of mixing varied. The lower boundary of the diurnal surface layer separated two distinct mixing regimes, the diurnal surface layer and the thermocline. Within the diurnal surface layer (which extended to 10- to 35-m depth), turbulent kinetic energy dissipation rates ε varied relatively little. Although variations in surface layer depth coincided with the daily change in direction of air-sea surface buoyancy production of turbulent kinetic energy (or simply, the surface buoyancy flux), ε was significantly greater relative to the buoyancy flux than was expected for a simple convective layer. In the thermocline below the diurnal surface layer, ε was highly intermittent; the day-night cycle was stronger, and variability was enhanced by turbulent "bursts" of 2–3 hours duration, which may be related to internal wave breaking events. The turbulent heat flux crossing 20-m depth was almost equal to the surface heat flux less the irradiance penetrating below 20 m. Seventy percent of the surface heat flux was transported vertically to the water below 30 m by turbulent mixing. Only a negligible amount penetrated to the core of the Equatorial Undercurrent. The gradient Richardson number Ri distinguishes between statistically different mixing environments. However, ε cannot be predicted from the value of Ri, since the intensity of mixing depends on the intensity of forcing in a way not specified by the value of Ri alone.

1. INTRODUCTION

At the equator, the South Equatorial Current (SEC) flows westward at speeds as high as 100 cm s^{-1} over the eastward flowing Equatorial Undercurrent (EUC). The EUC is driven at speeds as high as 150 cm s^{-1} by the basin-wide zonal pressure gradient set up by the westward wind stress [*McCreary*, 1981]. The signature of the zonal pressure gradient is an upward slope from west to east of the thermocline, in which the core of the EUC is embedded. In November 1984, at 140°W in the Pacific, the EUC core was about 120 m deep. Although the upper equatorial ocean is stratified, the vertical current shear above the EUC is large enough to reduce the gradient Richardson number Ri to values less than 1 [*Gregg et al.*, 1985; *Moum et al.*, 1986*b*; *Chereskin et al.*, 1986]. This combination of consistently small Ri and large stratification results in a mixing regime which may be unique to the equatorial ocean.

Turbulent mixing at the equator may make significant contributions to large-scale budgets. *Crawford and Osborn* [1979, 1981] suggested that the rate of dissipation of turbulent kinetic energy, ε, at the equator is the dominant sink in the energy budget of the EUC. The turbulent heat flux directed downward at 25-m depth is similar in magnitude to the flux of heat into the surface from the atmosphere [*Gregg et al.*, 1985]. The role of turbulence in transporting momentum seems to be complicated by the effects of internal waves [*Dillon et al.*, 1988].

Before the Tropic Heat experiment of 1984, studies of turbulence at the equator consisted of a few sets of sparse data [*Gregg*, 1976; *Crawford and Osborn*, 1979, 1981; *Moum et al.*, 1986*b*]. Because of other demands for station time on previous cruises and because of the nature of the instruments used to collect the data, none of these studies resulted in a continuous time series. The first systematic data set, obtained on the Tropic Heat I cruise of November–December 1984, yielded new insight into the processes determining turbulent mixing at the equator. Most importantly, we observed the characteristics and the intensity of the turbulence to change systematically in time. Large diurnal changes in ε (2 decades) were linked closely to changes in sign of the surface buoyancy flux [*Moum and Caldwell*, 1985; *Gregg et al.*, 1985]. The diurnal mixing cycle was further modulated by changes in the winds [*Moum and Caldwell*, 1985], possibly by meridional currents associated with large-scale waves and by the passage of a 4-day pulse, which depressed the EUC core, reduced the mean shear above the core, and significantly increased Ri [*Chereskin et al.*, 1986].

In this paper, we examine in detail the turbulent mixing at the equator as revealed by the data from Tropic Heat I. We observed two distinct regimes, separated vertically:

1. In the weakly stratified diurnal surface layer, changes in the intensity of mixing (ε) followed closely the day-night change in sign of the surface buoyancy flux. This layer was defined by the density step at its base, which cycled between 10 m (daytime) and 35 m (nighttime). Within the surface layer, the probability distribution of ε followed the lognormal form, with a relatively small standard deviation. Daily averages of ε varied by only a factor of 2. The 12-day average of ε was approximately twice the surface buoyancy production of turbulent kinetic energy, or about 3 times the value expected in a purely convective layer (in comparison to the results presented by *Shay and Gregg* [1986]). Also in contrast to a convectively mixed layer, which is truly well mixed, the observed equatorial surface layer was stratified.

2. In the well-stratified thermocline, turbulent "bursts" with lifetimes of 2–3 hours occurred at night, were separated in time by several hours, and persisted many hours past sunrise. Daily averages of ε varied by a factor of 10. We suspect that these bursts are linked to high-frequency internal waves. This region extended from the base of the surface layer to approximately 85-m depth.

Experimental details are discussed in section 2. In section 3

Paper number 88JC03788.
0148-0227/89/88JC-03788$05.00

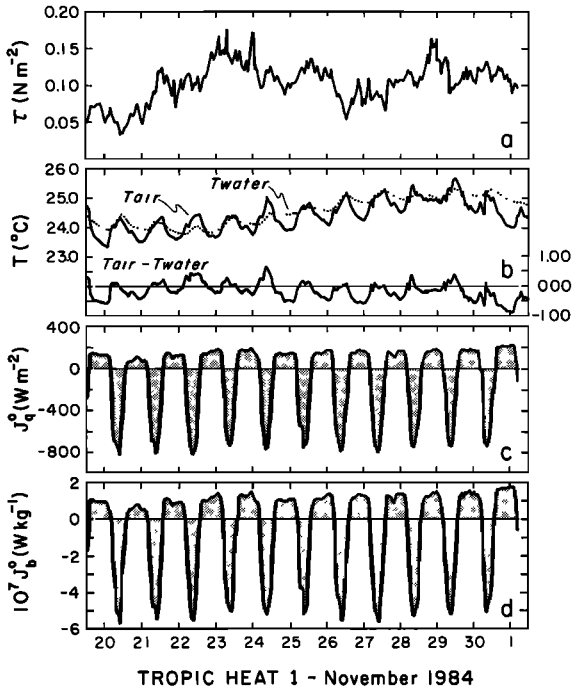

Fig. 1. Meteorological conditions during the 12-day observation period of Tropic Heat I (November 1984). (*a*) Wind stress τ in newtons per square meter, from winds measured at mast height on the R/V *Wecoma*. (*b*) Air temperature measured from the R/V *Wecoma*, water temperature taken from the ship's sea chest at 3-m depth, and the difference between these 2 values. (*c*) Net flux of heat at the sea surface, J_q^0, in watts per square meter. The daily heat input to the surface is dominated by shortwave solar radiation and is negative. The nighttime loss of heat from the surface is primarily latent heat and is positive. (*d*) Net flux of buoyancy at the sea surface, J_b^0, in watts per kilogram. Positive buoyancy flux is out of the sea surface (mass into the sea surface).

we present the meteorological and oceanographic conditions. The vertical structure of the mixing during the diurnal cycle is examined in section 4. Differences in mixing regimes in the surface layer and thermocline are characterized by their probability distributions in section 5. The importance of turbulent mixing in determining the local heat budget is discussed in section 6 (together with a comparison of methods for estimating the eddy diffusivity). A discussion of mixing parameterization (section 7) is followed by a general discussion (section 8) and summary (section 9).

2. Experimental Details

The experiment was designed to identify the processes responsible for upper ocean mixing at the equator and to determine the time scales of those processes. We profiled with the rapid sampling vertical profiler (RSVP) [*Caldwell et al.*, 1985] as continuously as possible. While keeping station near the Equatorial Pacific Ocean Climate Studies (EPOCS)/Tropic Heat T44 buoy (0°2'S, 140°9'W), we maintained nearly continuous 24-hour profiling from November 19 to December 1, 1984, obtaining 1749 profiles to 150-m depth of ocean microstructure data (temperature, conductivity, and small-scale shear), at the rate of 6–10 profiles per hour.

Estimates of currents relative to the ship, obtained from a hull-mounted acoustic Doppler current profiler (ADCP) [*Chereskin et al.*, 1987], were converted to absolute currents by referencing to the 200-m T44 current meter. Standard meteorological parameters (winds, humidity, solar and infrared radiation, air temperature, and sea surface temperature and conductivity) were recorded.

3. Background Conditions

3.1. *Meteorological Conditions*

Winds during the experiment averaged 8.9 m s^{-1}, a value considerably larger than the annual mean (e.g., 5.5 m s^{-1} for 1979–1980 (D. Halpern, personal communication, 1985) and also larger than means for other Novembers (e.g., 6.9 m s^{-1} during November 1979). Hourly mean winds varied from 5 m s^{-1} to 11 m s^{-1}. Hourly averages of the wind stress (calculated as $\tau = \rho_a C_D U_{10}^2$, where $\rho_a = 1.25$ kg m^{-3}, $C_D = 0.0012$ [*Large and Pond*, 1981], and U_{10} is the wind at 10-m height) varied from 0.03 to 0.17 N m^{-2} (Figure 1).

Sea surface temperatures (SST) measured from the sea chest of the R/V *Wecoma* (3-m depth) indicated two trends: (1) a 0.5°C diurnal variation and (2) a 1.25°C warming, due to northward advection of warm surface water by a 20-day meridional current oscillation [*Chereskin et al.*, 1986]. Air temperature followed SST closely, with a 1°C diurnal variation. The air also warmed as the advected surface water passed. Air-sea temperature differences never exceeded 1°C.

The surface heat flux J_q^0 (Figure 1) was estimated using bulk aerodynamic formulae [*Large and Pond*, 1981] and direct measurements of incoming solar and infrared radiation. Reflected solar radiation was estimated using the climatological value for albedo at the equator (0.06 [*Payne*, 1972]), and outgoing infrared radiation was estimated by use of the Stefan-Boltzmann law with emissivity equal to 0.97. The total surface heat flux was determined mainly by two factors, the incoming solar radiation (negative, representing a net flux of heat into the sea) and the latent heat flux (positive, representing heat out of the ocean). There were few clouds, and the daily solar heating remained relatively constant (Table 1). Nighttime cooling of the ocean surface varied by less than a factor of 2. Rainfall was negligible.

The surface buoyancy flux J_b^0 was estimated [*Dorrestein*, 1979] from the heat flux and evaporation estimates. In this case, a negative buoyancy flux represents an upward flux of mass (i.e., a downward flux of buoyancy). Solar radiation was assumed to be absorbed at the surface (we estimate from Secchi depth measurements that 86% was absorbed in the upper 20 m). Within a given day, J_b^0 varied from -6×10^{-7} W kg^{-1} (daytime peak) to 1.5×10^{-7} W kg^{-1} (nighttime). Day-to-day variations were small (Table 1).

Daily averages of meteorological parameters (Table 1) reveal a limited range of variation. In contrast, during the Tropic Heat II experiment (March to May 1987) we observed wind speeds as low as 1 m s^{-1}, as well as many cloudy days with rain squalls [*Park et al.*, 1987*a*, *b*]. Because surface forcing varied little from day to day, the 1984 data set lends itself to a study of the effect on upper ocean mixing due to variation of surface fluxes within the daily cycle.

3.2. *Oceanographic Conditions*

Oceanographic conditions during the experiment have been described by *Chereskin et al.* [1986]. Measurements were made mostly during the northward phase of a 20-day oscillation in the meridional velocity component. Two years of moored current meter data (from the T44 mooring (D. Halpern, personal communication, 1985)) indicate that the No-

TABLE 1. Daily Averages of Wind Stress τ, Net Surface Heat Flux J_q^0, Nighttime Surface Buoyancy Flux J_b^0, Averaged ε Between 10 m and the Mixed Layer Depth, and Averaged ε Between the Mixed Layer Depth and 85 m

	τ, N m^{-2}	J_q^0, W m^{-2}	$10^7 J_b^0$, W kg^{-1}	$10^7 \varepsilon_{MLD}^{10}$, m^2 m^{-3}	$10^7 \varepsilon_{85}^{MLD}$, m^2 s^{-3}	$10^7 u_*^2 dU/dZ$, W kg^{-1}
Nov. 20	0.59	−143	0.91	2.2	0.85	11.0
Nov. 21	0.69	−167	0.62	2.0	0.28	7.5
Nov. 22	0.11	−150	0.97	2.8	0.98	12.0
Nov. 23	0.13	−109	1.1	3.2	2.6	13.0
Nov. 24	0.13	−103	1.2	3.4	2.6	15.0
Nov. 25	0.11	−112	0.96	1.5	2.3	13.0
Nov. 26	0.11	−122	1.1	2.3	1.4	12.0
Nov. 27	0.08	−126	1.2	1.7	0.88	11.0
Nov. 28	0.10	−110	1.2	2.1	0.91	15.0
Nov. 29	0.13	−104	1.2	2.7	1.1	12.0
Nov. 30	0.11	−76	1.2	2.2	1.8	11.0
Dec. 1	0.11	−63	1.5	2.2	1.7	6.3
Cruise average	0.10	−115	1.1	2.3	1.4	12.0

The depth of the mixed layer has been defined by the $0.01\sigma_t$ difference from the sea surface. Negative J_q^0 is into the sea. Positive J_b^0 represents a mass flux into the sea.

vembers of both 1983 and 1984 were periods of energetic activity in the 20-day band. The surface expression of the oscillation was the 1.25°C warming (Figure 1) accompanied by a salinity increase of 0.3 psu, (practical salinity units; 1 psu = 1‰ salt by weight). These factors combined to produce a mean decrease in density corresponding to 0.2 σ_t at the sea surface (Figure 2). Meridional currents changed from weakly southward on November 19 to strongly northward (> 50 cm s^{-1}) in the upper 80 m by November 24, returning to weak southward flow by December 1.

A north-south transect from 3°N to 3°S along 140°W completed just before the 12-day experiment [*Moum et al.*, 1986*a*] indicated the width of the EUC to be about 2°, centered just north of the equator. Estimates of ε averaged 100 m vertically over the 6° transect did not define an obvious peak in turbulent mixing associated with either the equator or the EUC. Rather, variation of upper ocean ε along the ship's track was dominated by diurnal variability.

Variations in hydrographic parameters and currents during the 12-day observation period occurred on two time scales (shorter than the 20-day wave). The semidiurnal tide dominated the spectra of velocity fluctuations in both components, as well as the spectra of displacement of isopycnal surfaces below the surface layer, but ε was not correlated with these tidal oscillations. A large-amplitude pulse, which depressed the velocity maximum and the pycnocline by 30 m over a 2-day period during the experiment, did affect ε significantly. During the passage of the pulse, EUC core velocities decreased and the separation between surface and core increased, so that vertical shear was reduced and mean gradient Richardson numbers were increased. Lower values of ε accompanied the reduced shear and elevated Richardson numbers. Since the pulse arrived during the weakest winds of the experiment, it is impossible to determine which factor caused ε to be smaller.

The dominant variation in turbulent mixing (ε) was associated with daily changes in direction of the surface buoyancy

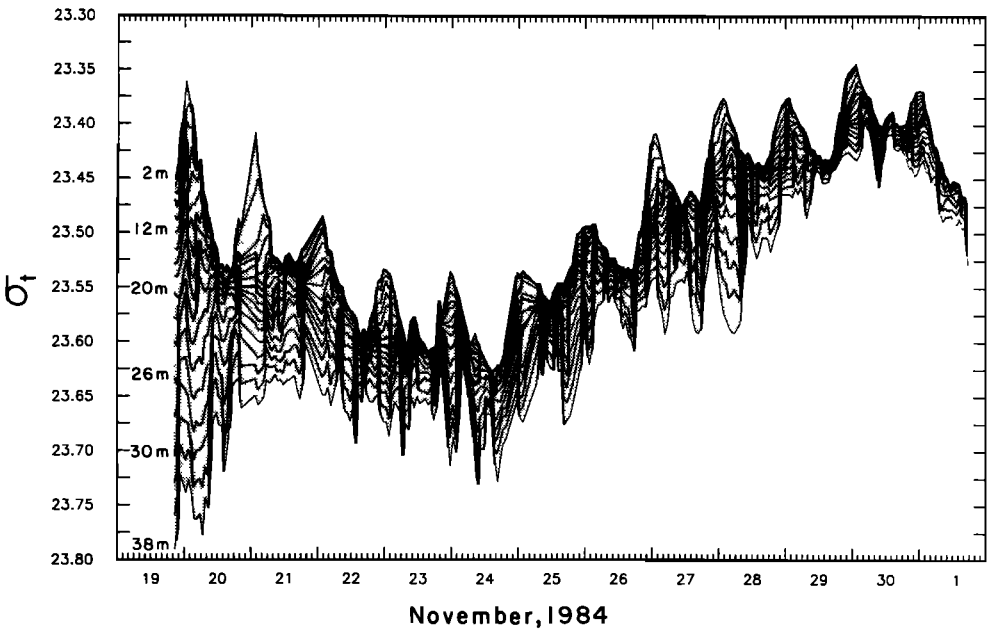

Fig. 2. Plot of σ_t at 2-m intervals from 2 m to 36 m.

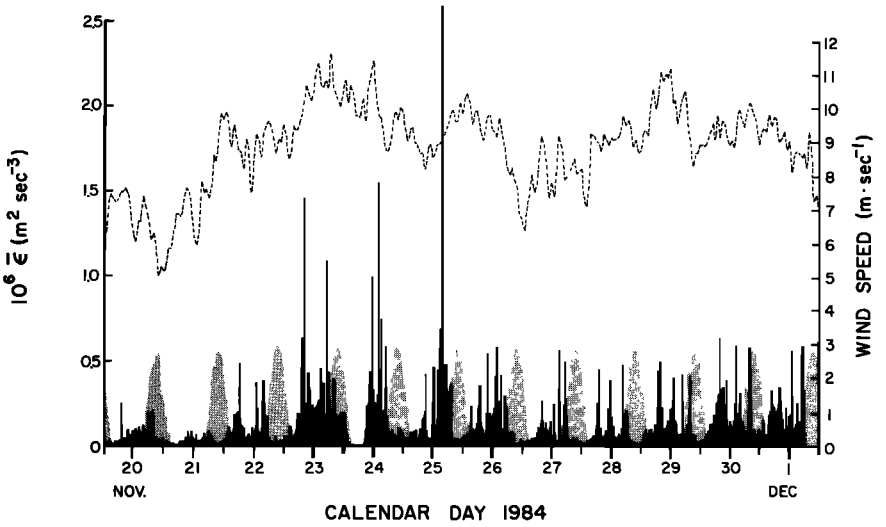

Fig. 3. Depth averaged ε (10–110 m) indicating the very clear diurnal signal in mixing. The large ticks on the abscissa represent 0000 UT (0200 LT). The stippled areas represent shipboard measurements of incoming solar radiation (peak values of 1000 W m^{-2}). Hourly winds from shipboard measurements are superimposed.

flux (Figure 3) [*Moum and Caldwell*, 1985]. The daily variation in density due to the mixing cycle was 0.05 σ_t units. This variation extended to at least 36-m depth at peak winds (Figure 2). In 12-day means computed for each hour of the day, ε differed by nearly a factor of 10, on average, between local noon and early morning (Figure 4), increasing through the night and decreasing suddenly several hours after sunrise. Daytime profiles show decreases in ε of more than a factor of 100 from profiles made the previous night. The process is not simple convective mixing as observed at mid-latitude sites [*Shay and Gregg*, 1986], since (1) the equatorial diurnal surface layer was weakly stratified, not well mixed, (2) ε was too large by a factor of 3 to be due to the measured surface buoyancy production of turbulent kinetic energy, and (3) ε followed this cycle in the thermocline. Although the surface buoyancy flux was not sufficient to force the observed mixing, the change in direction of the surface buoyancy flux apparently triggered the diurnal mixing cycle.

4. Diurnal Progression

4.1. *Typical Profiles*

The vertical structure of currents varied in response to the 20-day oscillation, the 4-day pulse, semidiurnal tides, and, presumably, other effects not resolved by our experiment. Typical profiles from November 28 at 0000 UT (1500 LT; Figure 5) and 1210 UT (0310 LT; Figure 6) reveal a well-defined EUC core at 105- to 120-m depth with maximum eastward currents of 140 cm s^{-1}, a weak westward current of 10 cm s^{-1} at 20-m depth, and a northward current greater than 60 cm s^{-1} above 50 m. In the profile of the magnitude of vertical current shear, $S = [(\partial U/\partial z)^2 + (\partial V/\partial z)^2]^{1/2}$, the EUC core appears as a local minimum.

The core of the EUC coincided with both the pycnocline and the salinity maximum (Figures 5*a* and 6*a*). The depth of the core was highly correlated with the depth of the $\sigma_t = 25.5$ density surface at time scales greater than 1 hour [*Chereskin et al.*, 1986]. Below the core, numerous intrusions were observed. For example, compensating temperature and salinity gradients in the warm, salty intrusion at 125-m depth in Figure 6*a* resulted in a layer of constant density. This intrusion also appears 12 hours earlier in Figure 5*a*. If this feature was advected by the 100 cm s^{-1} flow at the depth of the intrusion, its zonal length scale was greater than 40 km.

The local buoyancy frequency N (Figures 5*a* and 6*a*) increased from 3–4 cph at 18-m depth (depth bins were chosen to coincide with the depth bins of the ADCP shear estimates) to 10 cph at 100 m and decreased again below the EUC core. The gradient Richardson number, $Ri = N^2/S^2$, was less than 1 above the EUC core (frequently less than 1/4). Ri increased to a maximum (>10) at the depth of the velocity maximum (shear minimum) of the EUC. Below the core it decreased again, but only to a value of 1. The cruise-averaged profile of Ri is not significantly different from those shown in Figures 5*c* and 6*c* and is typical of profiles found in other equatorial experiments [*Gregg et al.*, 1985; *Moum et al.*, 1986*b*].

In the daytime the surface layer was warmed by solar heating (Figure 5) so that the stratification at 12 m was significant ($N = 4$ cph). At night the surface layer extended to at least 18 m (Figure 6; approximately 3 hours before sunrise), as is indicated by the step in the density profile. In spite of the daily variation in stratification in the upper layers, daily variations in shear balanced the stratification's contribution to Ri, with the result that we observed no diurnal variations in Ri at any depth [*Chereskin et al.*, 1986].

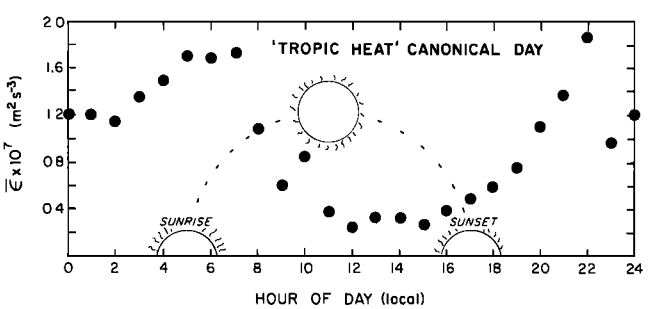

Fig. 4. Ensemble averages of depth-averaged ε (10–100 m) for each hour of the day over the 12-day experiment. The large value at 2200 LT is dominated by a burst of turbulence from a single night.

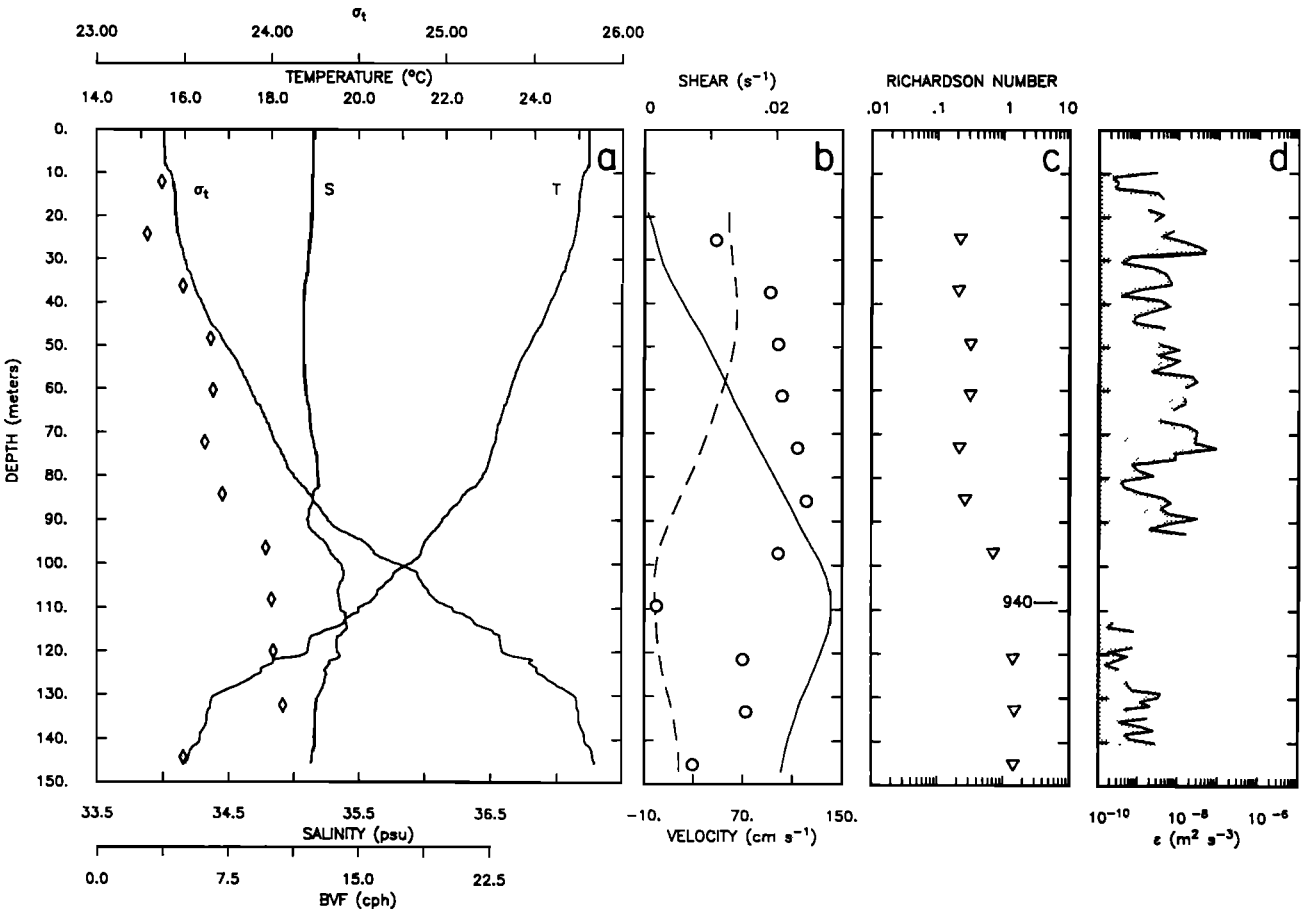

Fig. 5. Typical daytime profile of vertical structure (this profile was made at 0000 UT (1400 LT) on November 28 and is the first profile on the waterfall plot of σ_t shown in Figure 7). (*a*) Temperature, salinity, and σ_t. Temperature and salinity have been scaled to represent equal contributions to σ_t. Buoyancy frequency (diamonds) was computed over 12-m intervals to match the depth averaging interval of the ADCP-derived currents. BVF is Brunt-Väisälä frequency or buoyancy frequency. (*b*) Closest hourly average of east-west (solid line; east > 0) and north-south (dashed line; north > 0) currents as measured by the ADCP mounted on the hull of the R/V *Wecoma*. Shear magnitude (circles) was computed as $[(\partial U/\partial z)^2 + (\partial V/\partial z)^2]^{1/2}$, U and V being hourly averages. (*c*) Gradient Richardson number, $Ri = N^2/S^2$, where buoyancy frequency N and shear magnitude S have been vertically averaged to match scales. (*d*) Estimates of ε computed from 512-point spectra. The upper 10 m may be contaminated by ship wake, and estimates of ε are not plotted. Narrow band spectral contamination due to cable strumming in the strong equatorial currents affected the shear probe signals at depths of 110 to 130 m, and the ε estimates are not shown for these depths.

4.2. *Turbulent Bursts Below the Surface Layer*

Below the surface layer, turbulent dissipation rates were 100–1000 times larger at night than during the day (Figures 5*d* and 6*d*). Although the turbulence was highly intermittent and daytime ε values were occasionally as large as nighttime values ($>10^{-7}$ m^2 s^{-3}), large daytime values of ε occurred only over small vertical scales and short time scales. On the other hand, within the surface layer, nighttime values were consistently large for the entire period of positive buoyancy flux. In the well-stratified zone (N = 5–8 cph) below the surface layer, occasional nighttime bursts of turbulence persisted over several hours and several tens of meters vertically. Large-scale overturns between 35 and 55 m (Figure 6) were observed at night in varying stratification ($N \simeq 4$ cph at 36 m to $N \simeq 7$ cph at 60 m) and were associated with large values of ε ($\varepsilon > 10^{-6}$ m^2 s^{-3} at 50 m).

Twenty-four hours of density profiles (Figure 7) reveal a single nighttime deepening sequence in detail. The diurnal step at the base of the upper surface layer was a consistent feature allowing a surface layer depth to be defined. The deepening of the surface layer after sunset ($\simeq$0300 UT) was accompanied by three large mixing events in the well-stratified zone at the base of the surface layer (25 to 50 m), each lasting several hours and separated in time by several hours (0600–0800, 1100–1230, 1630–1830 UT). Each burst was marked by vigorous overturning and large values of ε (Figure 7*b*). Between bursts the water column restratified ($N \simeq 5$ to 7 cph). The relatively low value of N (2 cph) at 48 m in Figure 6*a* was temporary, the result of a burst (this profile comes from the second nighttime burst in Figure 7).

Turbulent bursts occurred on most nights (Figure 8). Our definition of mixed layer depth (MLD) defines a surface layer in which the variation in ε was small. Below the surface layer during the day, ε was smaller than could be displayed on the linear scale of Figure 8. In the surface layer at night, steady mixing was observed. Below the surface layer, intermittent bursts of turbulence were observed every night. These extended as deep as 85 m. On at least one occasion (November 30) a turbulent burst in the well-stratified zone occurred many hours past sunrise, extending from 40 to 80 m depth and

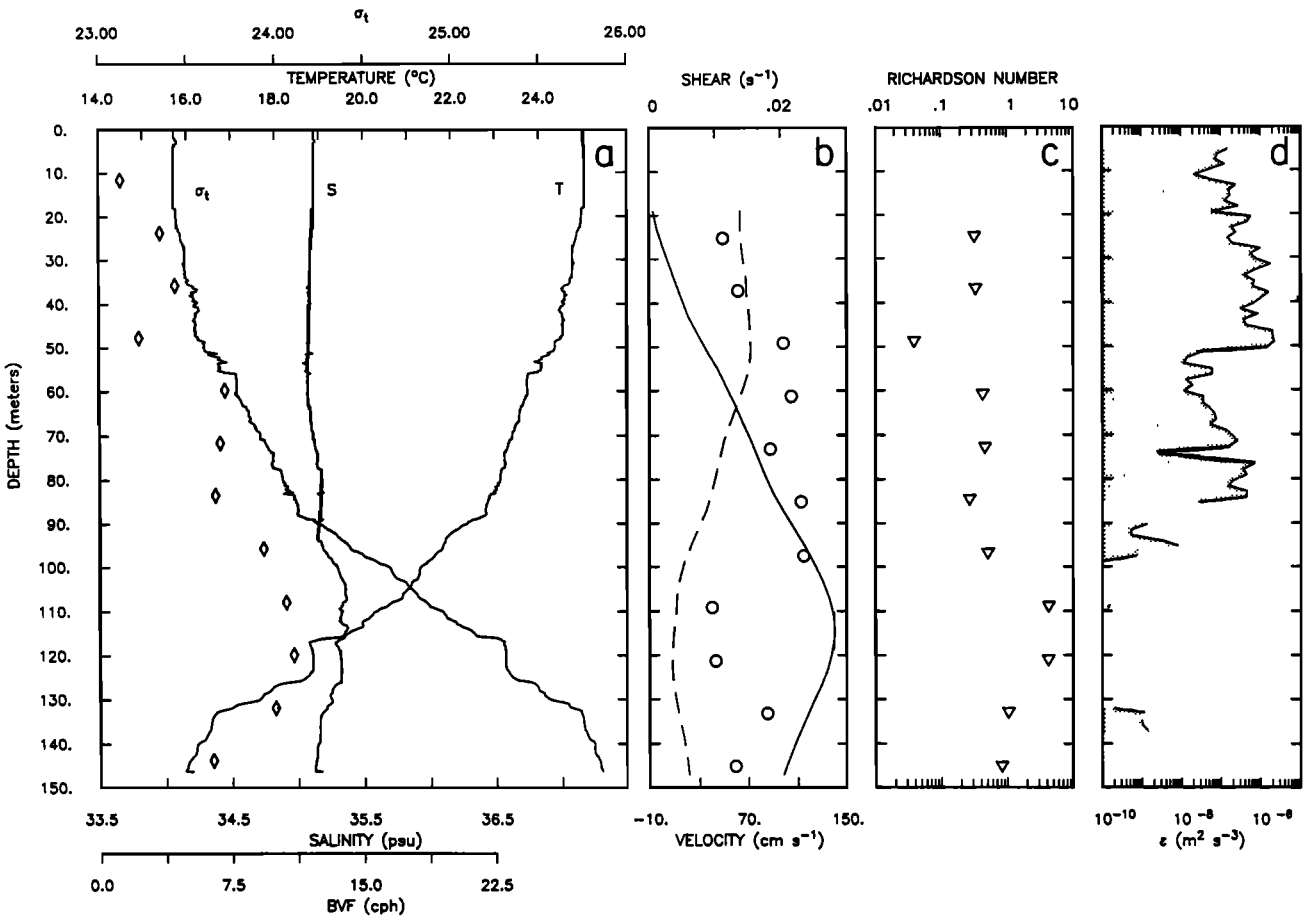

Fig. 6. Typical nighttime profile of vertical structure (1210 UT; 0210 LT on November 28). In relation to the waterfall plot of Figure 7 this profile was made during the second large burst of mixing below the surface layer base (see text). Symbols and scales are as in Figure 5.

persisting for 2–3 hours. Above this burst, ε was 100 times smaller; mixing did not extend continuously down from the surface. (Probability density distributions of surface layer ε are compared to those in the thermocline in section 5).

Because the mixing bursts lasted several hours and were separated by several hours, hourly averages of vertical profiles of ε resolved the significant mixing events (Figure 9). On several occasions, bursts occurred well past sunrise and did not extend all the way to the surface (November 20, 22, and 24, for example). Although the surface forcing seems largely to determine both the intensity and temporal variability of the mixing, there exist significant events which are not directly linked to the surface. Thus the coupling to the surface must be indirect and suggests an intermediary process not resolved by our measurements (we will later suggest the possible role played by internal waves).

4.3. *Daily Variability*

To characterize the vertical structure of mixing over the diurnal period, 5-m vertical averages of ε and N were computed for each hour of the day, and all those values falling within the same hour of day were averaged together (Figure 10); these will be referred to as $\langle\varepsilon\rangle$ and $\langle N\rangle$. The progression of the diurnal step in density is clearly seen in the $\langle N\rangle$ profiles. At sunrise, the profile of $\langle N\rangle$ is smooth ($\langle N\rangle \simeq 1$ cph near the surface) and no step is present. Three hours past sunrise the step is clearly seen. It develops, sharpens, and diffuses before sunset. Average values of $\langle N\rangle$ at 10-m depth exceed 3 cph by late afternoon. Late afternoon diffusion of the density step is likely linked to enhanced mixing observed in the upper 15 m. Past sunset the step moved downward, reaching 20-m depth 4 hours after sunset.

The full progression of the vertical structure of the mixing regime cannot be seen in the $\langle N\rangle$ profiles. The largest values of ε were observed below the surface layer, where complete restratification between bursts obscured the effect on ensemble-averaged $\langle N\rangle$ profiles. The deepening nighttime mixing layer is clearly seen in the $\langle\varepsilon\rangle$ profiles (Figure 10). Tagging the mixing layer by a threshold level ($\langle\varepsilon\rangle = 10^{-7}$ m^2 s^{-3}) is instructive. By late afternoon, intense mixing was confined to a thin layer near the surface. After sunset, mixing progressed downward ($\langle\varepsilon\rangle > 10^{-7}$ m^2 s^{-3} at 20 m at sunset and at 60 m by 5 hours past sunset). Below 60 m, only occasional bursts of turbulence penetrated (Figures 8 and 9) and did not have a great effect on ensemble averages. After sunrise, $\langle\varepsilon\rangle$ values were reduced near the surface, but large values of $\langle\varepsilon\rangle$ persisted at 40 m and below. Deep, persistent mixing events were common (Figure 9); the subsurface peaks in $\langle\varepsilon\rangle$ were not produced by single events.

The range in $\langle\varepsilon\rangle$ over the daily cycle at 5-m depth intervals is demonstrated by examining the transposed data of Figure 10 (Figure 11). Surprisingly, the diurnal variation in $\langle\varepsilon\rangle$ at 10-m depth was relatively small. By 15-m depth, the diurnal signal was clear and was apparent to at least 80-m depth. The

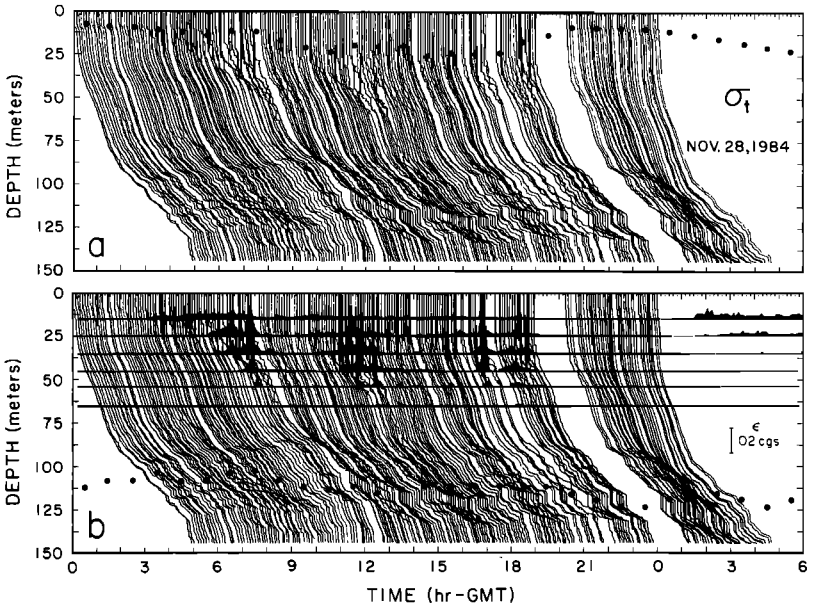

Fig. 7. (*a*) Waterfall plot of σ_t profiles from a single day (November 28) during the experiment. Profiles have been offset so that the surface point coincides with the time (UT) of the profile. Sunset was ≃0300 UT, and sunrise was ≃1500 UT. Time gaps in the series are due to instrumentation problems. The largest gap at 1900 UT coincides with our daily conductivity-temperature-depth profile during which microstructure profiling was suspended. Relative σ_t units are shown on the abscissa. Solid circles represent surface layer depth, defined by a 0.01 σ_t difference from the surface. (*b*) To the waterfall plot in Figure 7*a* have been added EUC core depth (solid circles; defined by zero zonal current shear) and 10-m-averaged ε for every profile of the day, displaced horizontally to match the σ_t profiles. Note the coincidence of the large and intermittent bursts below the surface layer base with the overturning density profiles. In contrast, ε within the surface layer is lower level and less intermittent.

variation in $\langle\varepsilon\rangle$ was largest at depths of 50 and 55 m (dynamic range of 100, compared to 10 at 15 m, 20 at 35 m, and decreasing below 55 m). At greater depths, the nighttime increase in $\langle\varepsilon\rangle$ occurred later. Judging onset of mixing by the time when $\langle\varepsilon\rangle$ first exceeded 10^{-7} m^2 s^{-3} following sunset, the lag with depth was approximately 1 hour per 5 m of depth to 50 m. Owing to greater variability and lower signal level below 50 m, the lag was not so easily quantified, but the daily peak in the mixing cycle below 60 m did occur considerably later.

5. STATISTICS OF ε

By increasing the quantity of data, recent technical advances in microstructure instrumentation have increased

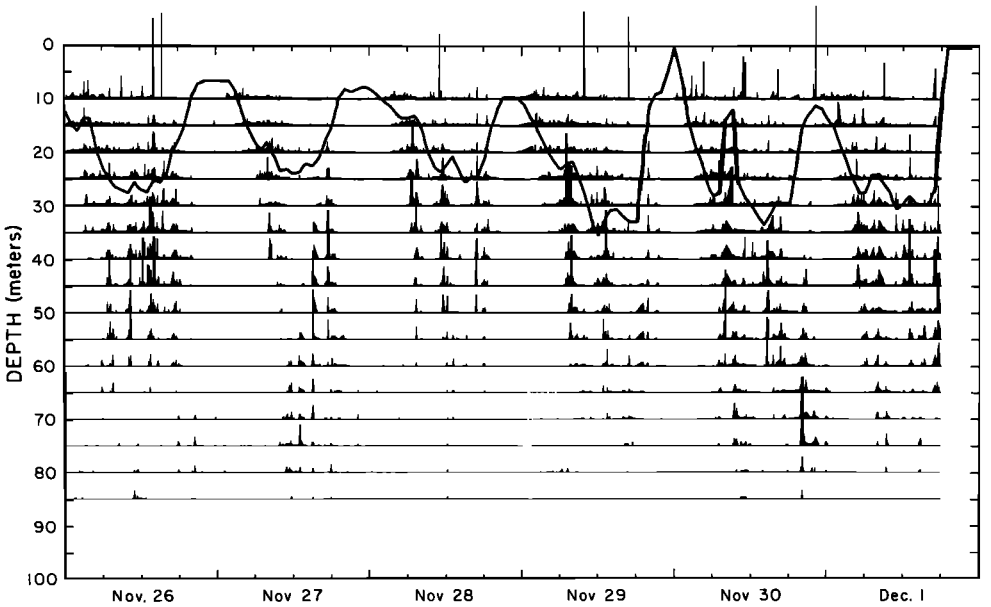

Fig. 8. Averages of ε over 5-m intervals, plotted as continuous time series over the latter 6 days of the observation period. The darker line represents the surface layer base. The uppermost series (centered at 10 m) has been averaged over 7.5 to 12.5 m and may occasionally be contaminated by ship wake or vehicle instability near the surface. Below the surface layer, ε was considerably more intermittent and exhibited greater dynamic range than within the surface layer.

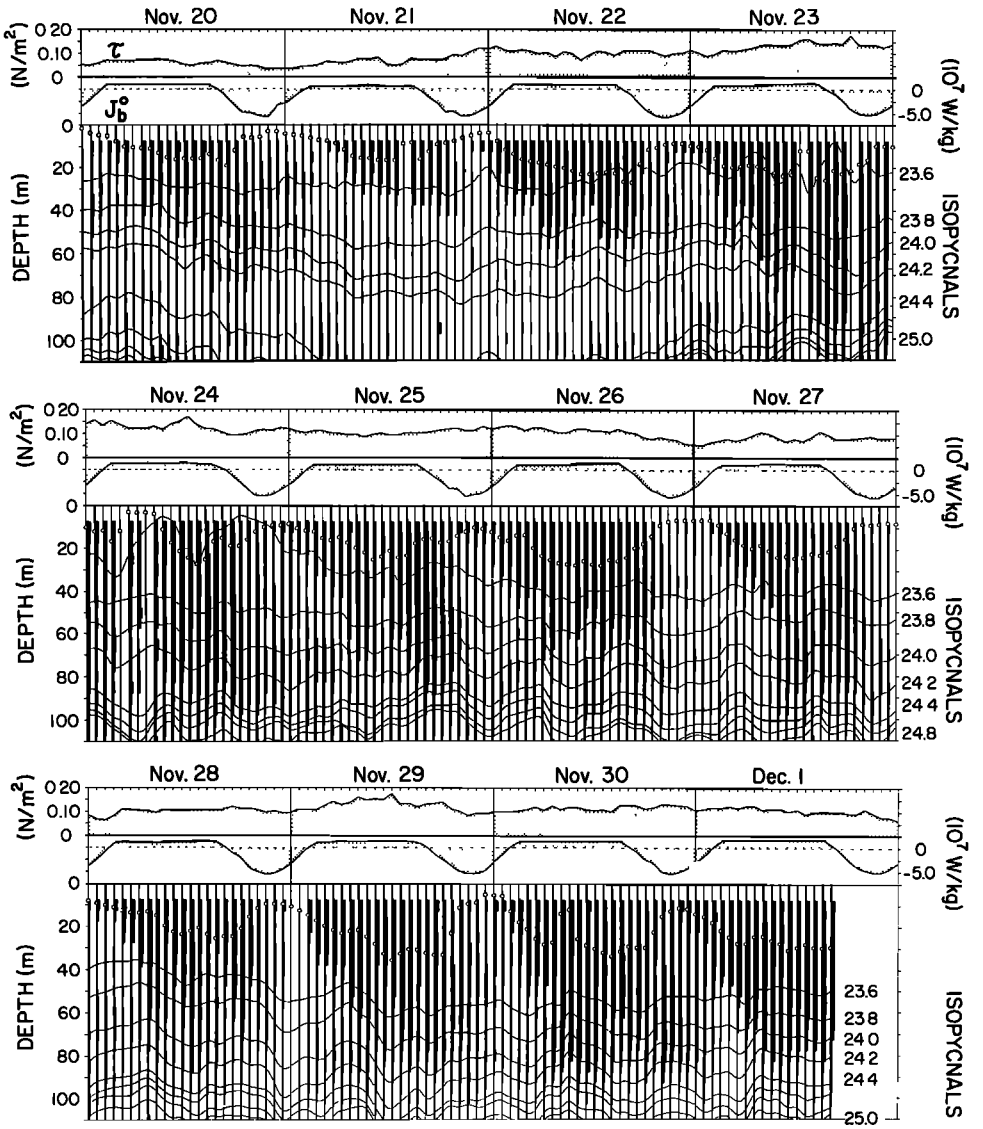

Fig. 9. Profiles of averages of ε over 1 hour and 5-m vertical intervals are shown for the entire experiment. The ε scale is 5 decades between vertical baselines, and the baselines are 10^{-9} m^2 s^{-3}. The profiles are presented in context of the surface forcing (wind stress, buoyancy flux), surface layer depth (open circles) and density surfaces. Occasional profiles (e.g., two profiles on November 23) showing negligible ε are due to a lack of observations during that hour.

greatly the confidence with which statistical distributions of microstructure quantities such as ε can be interpreted. For example, *Oakey* [1985] presented data from two upper ocean studies, averaged in vertical blocks of 10 to 15 m. *Osborn and Lueck* [1985*a*] examined a sample population drawn from a restricted depth range; 0.25-s estimates ($\simeq$0.25 m at their nominal speed of 1 m s^{-1}) of variance in measurements made using an array of sensors mounted on the research submarine USS *Dolphin*. *Osborn and Lueck* [1985*b*] also obtained a 1700-m horizontal sample (using a towed body) of 6.4-m averages of ε with a dynamic range of about 1 decade. *Shay and Gregg* [1986] studied two separate convective mixed layers in the upper ocean. In each case, reasonable agreement of the observed distributions in ε with the lognormal probability distribution was found, at least for some part of the distribution.

Monin and Yaglom [1975] argue that in a steady state turbulent flow, squared fluctuations like ε follow a lognormal probability distribution. The laboratory and geophysical studies reviewed by Monin and Yaglom seem to demonstrate lognormal distributions, at least over restricted ranges of the distributions. Whether or not the data in a given study were found in a steady state situation is difficult to assess. In most cases, measurements consist of single-point time series (in the laboratory and atmospheric boundary layer) or horizontal or vertical space series through a variable mean field (in the ocean). The trick is to restrict our attention to a regime that we might reasonably expect to be in steady state. The 1700-m horizontal patch observed by *Osborn and Lueck* [1985*b*] may be one such example, although the degree of stationarity of the process forcing the mixing is not clear. The convective mixed layers observed by *Shay and Gregg* [1986] were cases in which the mixing was driven primarily by the surface buoyancy flux. In these cases, the variation in $J_b{}^0$ was small, and ε scaled directly with $J_b{}^0$. The data from the convective mixed layers seem to exhibit the best fits to a lognormal distribution over the full range of the data.

For the Tropic Heat I data, probability density functions

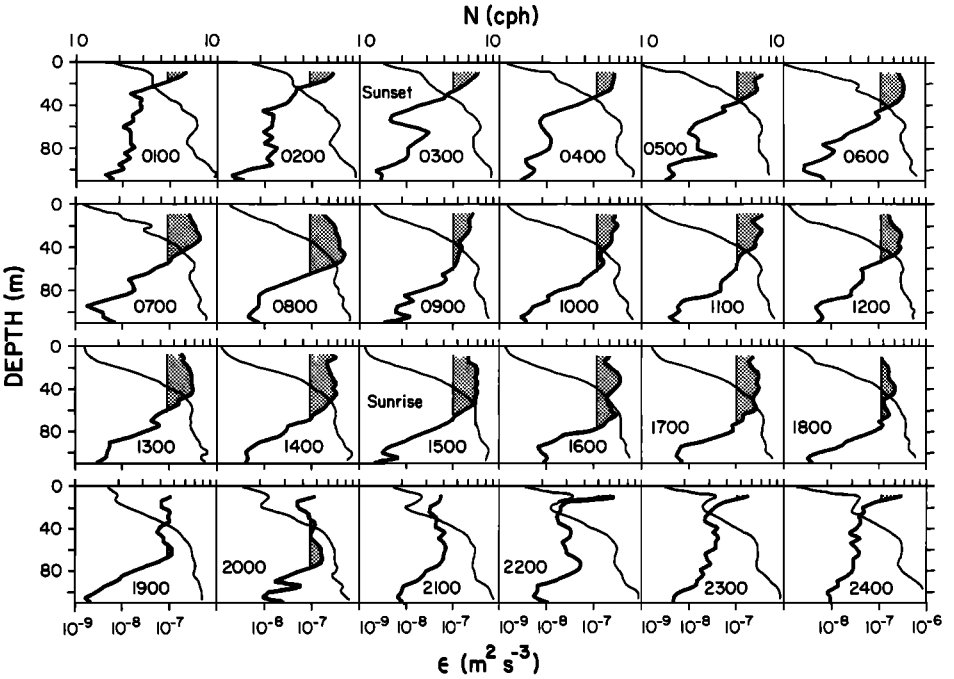

Fig. 10. Ensemble-averaged profiles of buoyancy frequency, N (light line) and ε (heavy line) in the upper 110 m. These have been constructed from 5-m vertical averages of N and ε for every hour of the day from each of the 12 days of the observation period. Values of $\varepsilon > 10^{-7}$ m^2 s^{-3} have been shaded. Hours of the day (UT) are shown in the bottom left-hand corner of each box. Sunset was approximately 0300 UT and sunrise was 1500 UT.

(pdfs) were computed separately for the two regions we have defined, surface layer and thermocline. Individual 512-point spectral variance estimates of ε (1- to 2-m vertical scale, depending on vehicle fall speed) were sorted.

The pdf for the surface layer (10 m–MLD; Figure 12*a*) is characterized by an arithmetic mean μ of 2.3×10^{-7} m^2 s^{-3} and a sample standard deviation σ of 3.8×10^{-7} m^2 s^{-3} ($\sigma/\mu = 1.64$). Between the surface layer and 85 m (MLD–85 m; Figure 12*b*), $\mu = 1.42 \times 10^{-7}$ m^2 s^{-3} and $\sigma = 3.94 \times 10^{-7}$ m^2 s^{-3} ($\sigma/\mu = 2.78$).

If ε is lognormally distributed, then $\ln(\varepsilon)$ is normally distributed with expected value $\mu_{\ln\varepsilon}$ and variance $\sigma_{\ln\varepsilon}{}^2$ [*Hines and Montgomery*, 1972]. These statistics were computed for each of the two cases and used to compute the corresponding lognormal probability distributions (plotted as dashed lines in Figures 12*a* and 12*b*). The expected value of ε, if lognormally distributed, is

$$E[\varepsilon] = \exp(\mu_{\ln\varepsilon} + \sigma_{\ln\varepsilon}{}^2/2) \quad (1)$$

Agreement of $E[\varepsilon]$ (MLE in Figures 12*a* and 12*b*) with the arithmetic mean is one indication of agreement with the lognormal distribution. For the surface layer data, $\sigma_{\ln\varepsilon}{}^2 = 1.1$; for the thermocline data $\sigma_{\ln\varepsilon}{}^2 = 4.8$. Not surprisingly, the surface layer data demonstrate a much better agreement with the computed lognormal distribution. However, the surface layer data failed a χ^2 goodness of fit test at all levels of significance ($\chi^2 = 83.2$ with 30 degrees of freedom). The problem is with the tails of the distribution. If we remove only the outermost 33 points (of 11,339) in the pdf of the surface layer data (most of which represent single occurrences) then the observed data fit the lognormal distribution according to a χ^2 goodness of fit test at the 75% significance level ($\chi^2 = 27.9$ with 28 degrees of freedom).

The effect of subdividing the data using the MLD as a boundary has been to produce one data set (surface layer) in which the effect of the diurnal cycle on the distribution of ε is effectively negated and one (thermocline) in which a strong effect of the diurnal cycle remains. Surface forcing (wind and nighttime surface buoyancy flux) remained reasonably steady

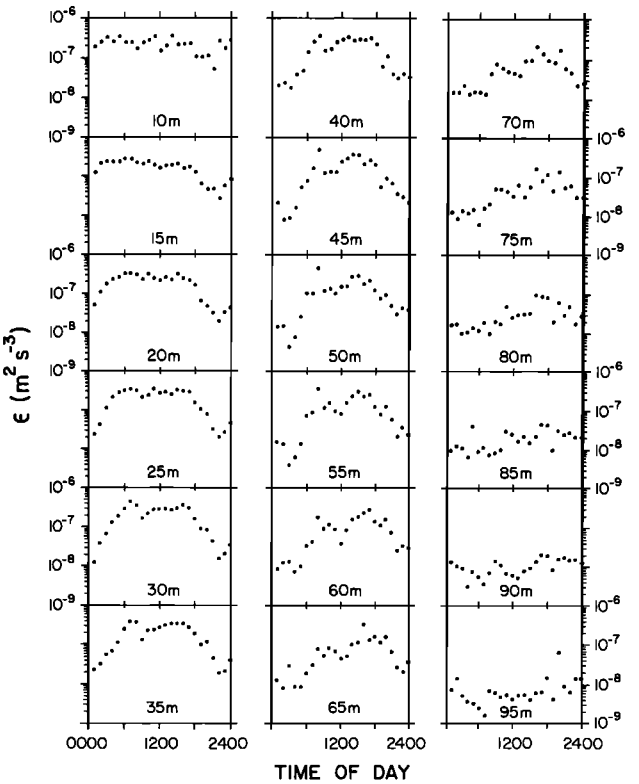

Fig. 11. Hourly ensemble averages of ε over 1 day (UT times) at 5-m depth intervals for the 12 days of the experiment. To construct this plot, the data points from Figure 10 have simply been transposed and replotted to show the averaged variation in ε within a daily cycle.

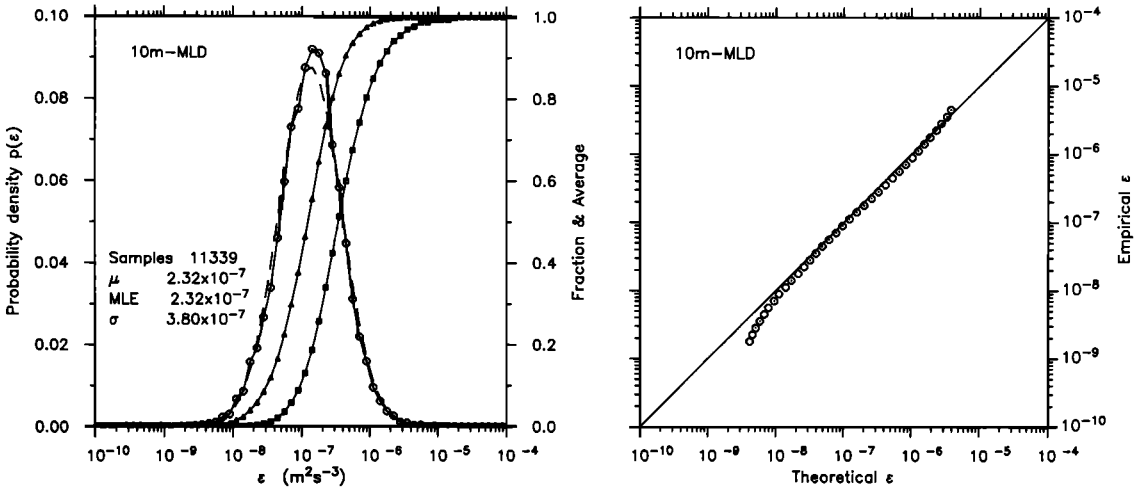

Fig. 12*a*

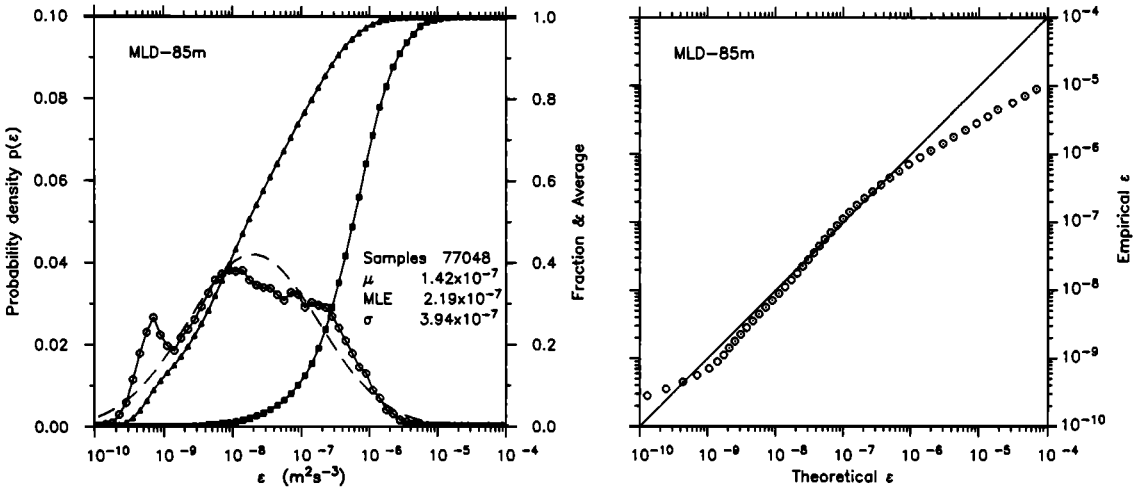

Fig. 12*b*

Fig. 12. (*a*) Probability density of ε (circles) over the depth range 10 m to surface layer base (MLD). Every 512-point spectral variance estimate of ε for the entire 12-day experiment was included (11,339 samples in the population). The arithmetic mean of ln ε, $\mu_{\ln\varepsilon}$, and sample variance $\sigma_{\ln\varepsilon}{}^2$, of the observed distribution were computed and used to construct the probability density of a lognormal distribution with $\mu_{\ln\varepsilon}$ and $\sigma_{\ln\varepsilon}{}^2$ (dashed line). MLE is the maximum likelihood estimator of the mean value of the lognormal distribution shown. Also shown are the cumulative distribution (triangles) and cumulative fraction of μ, the arithmetic mean of ε (squares). The sample standard deviation of ε is given by σ. In the right panel is shown the quantile-quantile (q-q) plot of the observed and lognormal-predicted values of ε for a given cumulative probability. The straight line (slope = 1) is for a perfect fit of the data to the lognormal distribution. Sample variance $\sigma_{\ln\varepsilon}{}^2 = 1.1$. (*b*) As for Figure 12*a* for the data included in the depth range MLD to 85 m (77,048 samples). Sample variance $\sigma_{\ln\varepsilon}{}^2 = 4.8$.

over the observation period. Surface layer ε was correspondingly steady (a variation of a factor of 2 in daily averages compared to a factor of 10 in daily averages from the thermocline). The small value of $\sigma_{\ln\varepsilon}{}^2$ indicates that we have defined a sample with limited dynamic range and perhaps one that might satisfy the steady state condition for which a lognormal probability distribution might reasonably represent the data.

Below the surface layer, the range in ε was much greater. Contributing to the pdf are variations on time scales of the diurnal mixing cycle and of the turbulent bursts.

6. Heat Budget

Before calculating eddy diffusivity and heat flux, we compared the results of using different methods of estimating these quantities from our data.

6.1. *Estimating* K_h

The vertical flux of heat due to turbulent mixing is defined by

$$J_q = \rho C_p \langle w'T' \rangle \tag{2}$$

where w' represents the vertical component of the turbulent velocity field, T' is the fluctuation temperature and angle brackets represent a suitable ensemble average (not usually attainable in practice; time averages are generally substituted). No direct measurements of $\langle w'T' \rangle$ have been made in the ocean, so several methods are used to infer the heat flux from measurable quantities (see recent reviews by *Caldwell* [1983] and *Gregg* [1987]). In the early days, the "Cox number" method was used exclusively. Its disadvantage is that it re-

quires full resolution of the vertical wave number spectrum of the temperature gradient. Because of the restricted time response of thermistors, the spectrum can be resolved only by limiting the fall speed of the vehicle to give the thermistor time to respond. Alternatively, a faster sensor might be used. Neither of these was routinely done on the Tropic Heat I cruise because a slow fall speed is impractical in the strong equatorial current shear and because no sufficiently fast-responding sensor is available that is also reliable enough to carry out long-term systematic sampling. Another method of estimating the vertical heat flux is based on shear measurements in the dissipation range. Shear sensors are sufficiently reliable and fast enough to resolve the shear spectrum at the fall speed required (1 m s^{-1}), so they were used for all of the casts. There is, however, some question about the magnitude of the coefficient involved in the dissipation method (see below). Therefore, microconductivity sensors fast enough to resolve the temperature-gradient spectrum were added on a subset of the casts in order to evaluate the dissipation method and to calculate its coefficient.

Osborn and Cox [1972] assumed that for steady and laterally homogeneous turbulent flow, the rate of production of temperature variance is balanced by the rate at which temperature variance is dissipated by molecular diffusion. The resulting form for an approximation to the eddy coefficient for heat diffusion is

$$K_h = \chi/2(\partial T/\partial z)^2 \tag{3}$$

where $\chi = 2\kappa\langle(\partial T'/\partial x_i)^2\rangle$, κ is the molecular diffusion coefficient for heat in seawater, and $K_h = \langle w'T'\rangle/(\partial T/\partial z)$. Our measurements allow us to estimate a single component, $\langle(\partial T'/\partial z)^2\rangle$, of $\langle(\partial T'/\partial x_i)^2\rangle$. We actually estimate $\chi = 2\kappa\alpha\langle(\partial T'/\partial z)^2\rangle$ where the value of α lies between 1 and 3, depending on the state of isotropy of the turbulence. The factor α has not clearly been established [*Caldwell*, 1983]. However, the energetic patches which dominate the mean values of turbulence quantities appear to be locally isotropic over the high wave number dissipation band [*Gargett et al.*, 1984]; hence it seems appropriate to use $\alpha = 3$ for energetic cases. A one-dimensional Cox number may be defined by $C_x = \langle(\partial T'/\partial z)^2\rangle/(\partial T/\partial z)^2$ so that

$$K_h = 3\kappa C_x \tag{4}$$

For a limited number of daytime profiles, we employed a four-electrode microconductivity probe [*Head*, 1983]. This sensor responds to conductivity fluctuations (due to a combination of temperature and salinity fluctuations) at wave numbers of up to 300 cycles m^{-1} [*Head*, 1983]. The signal was filtered at 240 Hz and sampled at 600 Hz for a Nyquist wave number of 300 cycles m^{-1} and filter attenuation of 3 dB at 240 cycles m^{-1} at our nominal fall speed of 1 m s^{-1}. Under certain conditions, this permitted full resolution of the temperature variance spectrum. However, the sensor was noisy, and its calibration drifted (more recent versions of the sensor have given better results). When the mean temperature gradient was large and mixing was energetic, so that the signal-to-noise ratio was acceptable, the temperature variance spectrum was well resolved, and confidence can be placed in estimates of C_x (because of sensor drift we have computed the dimensionless quantity C_x rather than χ). In several cases where the mean salinity gradient was also large, we observed spectral rises past the thermal diffusive cutoff which could be due to salinity variance. The scalar spectra of temperature and salinity are offset in wave number by the square root of the ratio of molecular diffusivities, $\simeq 10$, so that the two spectra may well be distinguishable under certain conditions. We found no examples, however, of well-resolved salinity variance spectra.

Another method for estimating K_h was developed to take advantage of the ability to estimate ε in the ocean [*Osborn*, 1980]. This approach requires a number of assumptions to reduce the turbulent kinetic energy equation to

$$P = J_b + \varepsilon \tag{5}$$

where $P = \langle u'w'\rangle\partial U/\partial z$ is the rate of production of turbulent kinetic energy by the Reynolds stress working against the mean shear and $J_b = -g\langle\rho'w'\rangle/\rho$ is the rate of destruction of turbulent kinetic energy by buoyancy. Defining K_ρ as $\langle\rho'w'\rangle/(\partial\rho/\partial z)$ and the flux Richardson number, R_f, as J_b/P, Osborn obtained the expression

$$K_\rho = R_f/(1 - R_f)\,\varepsilon/N^2 = \gamma\varepsilon/N^2 \tag{6}$$

Osborn concluded that the value of γ is less than 0.2, because of laboratory measurements indicating that R_f is less than 0.15. Recent laboratory measurements by *Rohr and Van Atta* [1987] indicate that 0.2 is a good estimate for γ in stratified flows with $Ri \geq 0.1$.

An analogous derivation yields an estimate for the eddy coefficient for momentum [*Gregg et al.*, 1985]. The relevant form of the turbulent kinetic energy equation is not clear, however, if internal waves play a critical role in the dynamics of the mixing process, since internal waves can transport momentum without transporting mass. This issue has been dealt with separately [*Dillon et al.*, 1988].

If the scalar mixing can be represented by a single turbulent diffusivity, i.e., if $K_h = K_\rho$, then it follows from (4) and (6) that

$$3\kappa C_x = \gamma\varepsilon/N^2 \tag{7}$$

To compare heat fluxes estimated by the Cox number method with those estimated by the dissipation method, we selected from those profiles which included microconductivity measurements 83 eddies of vertical scale 1 to 15 m. We included only those eddies for which (1) the upper and lower boundaries were clearly defined, (2) the mean temperature gradient was large enough that the microconductivity probe sensed signal above the noise, and (3) ε was above the noise level in the shear sensors. Most of these eddies came from the region below the surface layer (50–90 m) several hours past sunrise. For each eddy, the quantities C_x, N, and ε were computed. (Because the temperature-salinity relation was well defined over several hours and because σ_t was determined chiefly by temperature (Figures 5 and 6), the computation of N was made from the temperature measurement.) The mean vertical temperature gradient and N were computed from the stably reordered temperature profile. The resulting best straight line fit to the data yields

$$\kappa C_x = (0.1 \pm 0.06)\varepsilon/N^2 \tag{8}$$

Equating the two forms for the eddy diffusivity,

$$3\kappa C_x = 3(0.1 \pm 0.06)\varepsilon/N^2 \tag{9a}$$

or

$$0.12 \leq \gamma \leq 0.48 \tag{9b}$$

This result is no better, or no worse, than that obtained by *Oakey* [1982] using a similar method. Osborn's suggested

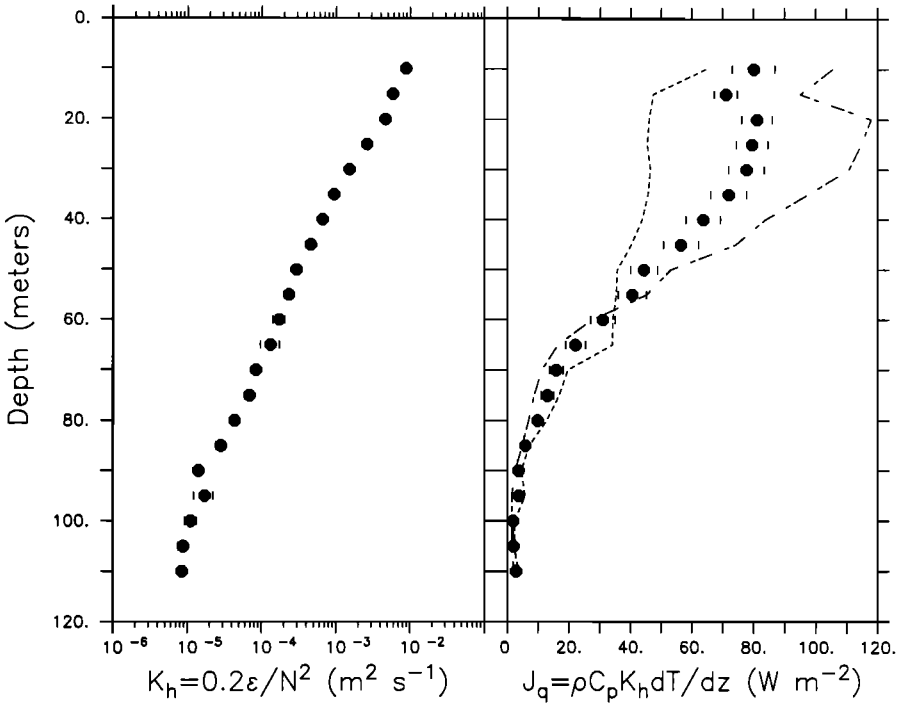

Fig. 13. Cruise-averaged vertical profiles of (left) eddy diffusivity for heat defined by $K_h = 0.2\varepsilon/N^2$ computed by averaging hourly K_h values, and (right) turbulent heat fluxes J_q computed from hourly values of $\rho C_p K_h\, dT/dz$, where ρ is the water density and $C_p = 4000$ J kg^{-1} K^{-1}. Confidence limits of ± 1 standard deviation of the mean were computed using a bootstrap test on the parent population of the 288 hourly averaged samples at each depth. Distributions of bootstrapped means were approximately Gaussian, and 68% of the values lie within the plotted confidence limits. Confidence limits not shown lie within the symbol (there were no instances where confidence limits were off the page). Also shown are nighttime (ensemble averaged over 1800 to 0600 LT; long- and short-dashed line) and daytime (ensemble averaged over 0600 to 1800 LT; dashed line) profiles of J_q.

value of 0.2 is within the range of uncertainty and is used here to estimate the turbulent heat fluxes.

6.2. *Local Heat Budget, Including Turbulent Fluxes*

Cruise-averaged values of K_h, estimated as $0.2\varepsilon/N^2$ (Figure 13; from hourly averages of ε and N) decreased approximately exponentially with depth from 10^{-2} m^2 s^{-1} at 10 m to 10^{-5} m^2 s^{-1} at 110 m, which is just above the EUC core. The turbulent heat flux

$$J_q = -\rho C_p K_h\, dT/dz \tag{10}$$

was computed from hourly averages of K_h and dT/dz, the local water density ρ, and a nominal value for the specific heat of seawater, C_p, of 4000 J kg^{-1} K^{-1} (Figure 13). The turbulent flux of heat downward from the upper 30 m was approximately 80 W m^{-2}. At night (1800 to 0600 local time), the average value of J_q at 30 m was 115 W m^{-2}, whereas it was 45 W m^{-2} during daylight hours. On the other hand, the daytime value of J_q below 60 m was more than twice the nighttime flux, because the deeper mixing events followed sunrise (Figures 9 and 10). Over the 12 days of the experiment, the net surface flux was -115 W m^{-2}, representing a gain of heat by the ocean. Seventy percent of that heat was mixed down to 30 m by turbulent processes, but only a negligible amount penetrated to the EUC core.

We computed the heat content per unit surface area in the upper 20 m as

$$H = \rho C_p \int_{-20}^{0} \{T\}\, dz \tag{11}$$

at 12-hour intervals (0600 and 1800 LT). These intervals give the maximum day-night difference in the upper ocean. *Imawaki et al.* [1988] show that the averaged temperature deviation below 25 m was very small compared with the daily temperature variations in the upper 20 m. This gives us confidence that we have eliminated the vertical motions induced by the internal tide in these averages. The time rate of change of the heat content, H_t, was computed by differencing hourly averaged temperature profiles at successive 12-hour intervals,

$$H_t = \rho C_p \int_{-20}^{0} \{(T[0600] - T[1800])/(12 \text{ hours})\}\, dz \tag{12}$$

The local heat budget is

$$H_t = J_q{}^0 - J_q - I_{20} - \rho C_p \int_{-20}^{0} \{uT_x + vT_y + wT_z\}\, dz + HD \tag{13}$$

We have estimated H_t, J_q and $J_q{}^0$ independently HD represents the contribution of horizontal diffusion. Mean values over the 12-day experiment are shown in Figure 14. I_{20} is the irradiance penetrating below 20 m. Secchi disk measurements on four cloudless days within 2 hours of local noon yielded Secchi depths of 22, 24, 26, and 26 m, for an average depth of about 25 m. According to *Paulson and Simpson* [1977], the irradiance has fallen to 10% of its surface value at Secchi depth. The average value of I_{20} during our experiment was 19 W m^{-2}.

The sum of advective terms and horizontal diffusion terms in the heat balance equation was estimated as the residual of the sum of the terms which were estimated directly (Figure

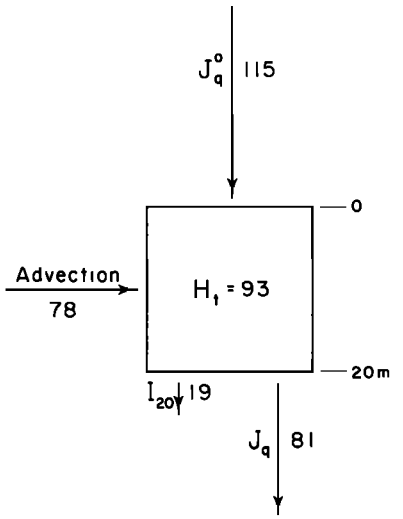

Fig. 14. Schematic showing terms in the heat budget estimated for the upper 20 m of the water column during the 12 days of the experiment. The local rate of change of the heat content, H_t, was computed by differencing the heat content estimated over successive 12-hour periods (0600 to 1800, and 1800 to 0600 LT) and averaging over the experiment. I_{20} is the irradiance penetrating below 20 m. The advective term was estimated as the residual of the other terms. The arrow lengths are proportional to the magnitude of each term.

14). The zonal advective heat flux cools rather than warms and cannot account for the increased heat content in the upper 20 m. Since temperature gradients are small in the upper 20 m, and since we expect vertical velocities to be small near the surface, we have considered the vertical advection of heat to be negligible. The advective residual (78 W m^{-2}) may be due completely to an influx of warmer water brought by the northward moving phase of the 20-day oscillation (Figures 1 and 2). The transect of RSVP profiles from 3°N to 3°S along 140°W just before the 12-day station indicated a 1°C horizontal temperature change over 100 km in the upper 40 m across the equator (warmer to the south [*Park et al.*, 1985]). Northward currents of 50 cm s^{-1} in the upper 20 m accompanied the 20-day oscillation [*Chereskin et al.*, 1986]. An average northward current of 20 cm s^{-1} over the duration of the experiment would be a reasonable estimate. This combination yields

$$\rho C_p \int_{-20}^{0} \{vT_y\}\, dz \simeq 160 \text{ W m}^{-2} \qquad (14)$$

which is sufficient to account for the advective residual. At 20-m depth, the surface heat flux J_q^0 is nearly balanced by the sum of J_q and I_{20}. H_t, then, is nearly equal to the advective contribution. It is possible that the southward moving phase of the 20-day oscillation contributes an equal amount of cooling, so that the net advection becomes insignificant when averaged over a full cycle of the oscillation.

7. ε AND Ri

One of the goals of the Tropic Heat program was the development of a relationship between turbulent mixing and quantities that are more easily measured. Such a relationship would be important (1) for observations, to make possible the estimation of turbulent fluxes from, for example, mooring data, and (2) for models, to provide subgrid-scale parameterization of turbulent processes. The common hypothesis is that mixing is related to the gradient Richardson number Ri, the ratio N^2/S^2 of the squared buoyancy frequency to the squared shear magnitude. Because a value of Ri of 1/4 is an instability threshold of the Taylor-Goldstein equation [*Miles*, 1961], it is often assumed that mixing results when Ri drops below 1/4 (some ocean measurements have suggested a lower threshold [*Eriksen*, 1978]). Specifically, modelers would like to know the vertical transports of heat and momentum due to turbulent mixing. An estimate of the eddy coefficient for vertical heat flux due to turbulence and the corresponding turbulent flux was discussed in the preceding section. The method requires estimates of ε and N. Since N is usually calculated in models, or measured by moored sensors, the most general approach we can take is to attempt a parameterization of ε so that the calculated or measured N might be used.

We have estimated Ri over various vertical scales (12 m in Figures 5 and 6) from the Tropic Heat data and compared the results with estimates of ε. Since ADCP velocities require time averaging to improve the signal-to-noise ratio [*Chereskin et al.*, 1986], we have chosen 1-hour averages of both Ri and ε for comparison.

The spatial sampling of S was quite different from that of N and ε. N and ε were calculated by averaging 6–10 profiles, acquired as the RSVP followed a vertical path, whereas S was calculated by vertically differencing ADCP profiles, the spatial averaging of which is complex. The ADCP return signal was averaged vertically over 12 m by the convolution of two gates, the range gate (6.2 ms) and the pulse length (20.4 ms). Horizontal averaging was included automatically in proportion to both the distance from the source (depth) and the cotangent of the angle of beam orientation. Any relationship between Ri and ε must be considered in light of these limitations. The noise in 10-min-averaged ADCP velocity estimates was 1 cm s^{-1}

We averaged ADCP shear vertically over 24 m. Hourly averages of N and ε (at 6–10 profiles per hour) were averaged vertically to match. Since the spatial scale of these averages is much larger than the scales of most turbulent eddies, we cannot address the physics of discrete mixing processes. In the following we examine the relationship between Ri and ε on scales which may be useful to equatorial modelers and observationalists; we also discuss the caveats associated with such a relationship.

The hourly, 24-m-averaged estimates of Ri and ε (Figure 15) covered four vertical bins: [27–51 m], [51–75 m], [75–99 m], and [99–123 m]. Because we expect that the mixing processes are completely different in the low N region near the surface from those in the stratified zone below, we excluded most of the data from the upper surface layer by starting at 27 m. The largest values of Ri in Figure 15 appear mostly in the bottom bin, accompanied by the smallest values of ε. For $Ri < 0.7$, the dynamic range in ε extends over $3\frac{1}{2}$ decades, from $< 10^{-9}$ m^2 s^{-3} to $> 10^{-6}$ m^2 s^{-3}.

Several tests were made to determine the effect of varying the averaging scheme:

1. Averaging time was varied from 1 hour through 2, 6, 12, 24, and full-station averages for the 12-day observation period. The effect was to reduce the dynamic range in ε, though not significantly in Ri. Averages of ε over fixed ranges in Ri did not change significantly, and the conclusions drawn in the discussion to follow would not change.

2. Vertical averaging was varied from 12 m through 24, 48, and 96 m. This effect was considerably more important, both in pushing the cutoff value to higher Ri and in changing the

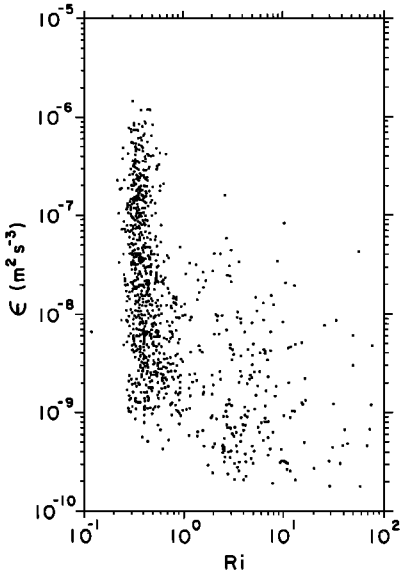

Fig. 15. Gradient Ri versus ε averaged to match scales of 24 m in depth and 1 hour in time for the entire 12-day observation period.

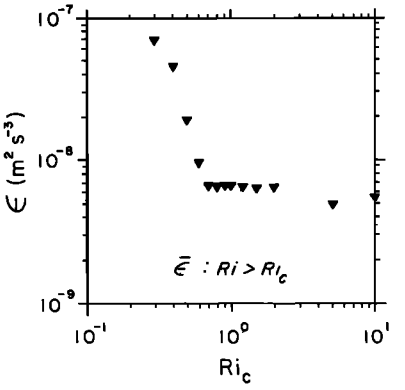

Fig. 16. Averaged ε as a function of Ri as an upper bound. All of the ε values in Figure 15 less than a given Ri have been averaged together. We use this computation to determine a cutoff Ri, Ri_c, which defines two distinct populations.

averaged ε in a given bin (i.e., the vertical variation was greater than the time variation).

The Ri-ε plot seems to represent a two-state process (Figure 15). The distribution of ε at small Ri is distinctly different from the distribution at large Ri. To choose a cutoff Ri, Ri_c, that represents the boundary between the two distributions, averages of ε for all $Ri > Ri_c$ were plotted versus Ri_c (Figure 16). The best choice of Ri_c is clearly $Ri_c = 0.7 \pm 0.05$.

Given a value for the Richardson number computed with the averaging described above, how do we best infer a value of ε? Our measurements suggest that we cannot with certainty predict ε from Ri. These measurements do suggest that if Ri exceeds Ri_c, ε is selected randomly from the distribution of Figure 17*b*, whereas if Ri is less than Ri_c, then ε is selected randomly from the distribution plotted in Figure 17*a*. At this point there is no indication of the degree of generality either of this concept or of the parameters involved (the value of Ri_c or the distributions themselves).

A possible method of obtaining K_h, then, might simply be to use the mean values of ε corresponding to Ri_c. For example, for $Ri < 0.7$, $\varepsilon = 9.2 \times 10^{-8}$ m^2 s^{-3} and $K_h = 1.8 \times 10^{-8}/N^2$ m^2 s^{-1}. For $Ri > 0.7$, $\varepsilon = 6.6 \times 10^{-9}$ m^2 s^{-3} and $K_h = 1.3 \times 10^{-7}/N^2$ m^2 s^{-1}.

Excluded from this discussion is a determination of the dynamics which drive the turbulence. Although the most energetic mixing occurred only at small Ri, we frequently observed instances of small Ri and small ε. Although small Ri is a condition necessary for mixing, the rate of mixing (magnitude of ε) must depend on the direct forcing of the turbulence at the time and place of the measurements. Hence with no further understanding of the forcing, it is impossible to generalize our result.

8. Discussion

8.1. *Diurnal Surface Layer*

Although changes in the thickness of the diurnal surface layer closely followed changes in the direction of the surface buoyancy flux (Figure 9), averaged values of ε in the surface layer were 3 times those expected in a purely convective mixed layer (Table 1). Whereas in the convective layers discussed by *Shay and Gregg* [1986], two from the ocean and one from the atmosphere, estimates of the ratio of the dissipation to the surface buoyancy flux lay between 0.61 and 0.72, in the Tropic Heat I surface layer that ratio was approximately 2.2. Furthermore, daily variations in surface layer ε were not correlated with variations in the nighttime buoyancy flux (Table 2; this is a fair comparison, since the surface layer was almost always less than 10 m when $J_b^0 < 0$). We conclude that this layer was not driven primarily by convective forcing.

Daily variations in surface layer ε were, however, correlated with the wind stress τ. To parameterize the production term in the turbulent kinetic energy budget, we have computed the sea surface friction velocity $u_* = (\tau/\rho)^{1/2}$ and the velocity shear between current meters at 10- and 25-m depth at mooring T44 [*Chereskin et al.*, 1986] and have used

$$u_*^2\, dU/dz = \langle u'w' \rangle dU/dz \qquad (15)$$

TABLE 2. Correlation Matrix of Daily Averages in Table 1

	$10^7\ \varepsilon_{MLD}^{10}$, W kg^{-1}	$10^7\ \varepsilon_{85}^{MLD}$, W kg^{-1}	$10^7\ J_b^0$, W kg^{-1}	τ, N m^{-2}	$10^7\ u_*^2\ dU/dZ$, W kg^{-1}
ε_{MLD}^{10}	1	0.42 (±0.37)	0.17 (±0.21)	0.63 (±0.18)	0.44 (±0.24)
ε_{85}^{MLD}		1	0.29 (±0.30)	0.71 (±0.15)	0.54 (±0.23)
J_b^0			1	0.50 (±0.18)	0.07 (±0.51)
τ				1	0.49 (±0.21)
$u_*^2\ dU/dZ$					1

Correlation coefficients were computed using the nonparametric bootstrap method: 1000 samples of size 12 were drawn with replacement from the parent population and statistics computed. The correlation coefficients are expressed as the mean value of the bootstrapped correlation coefficient (±1 standard deviation of the mean).

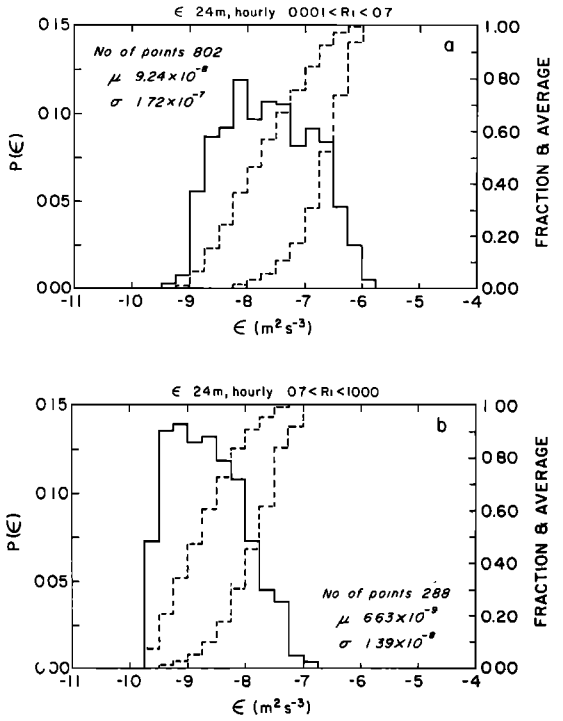

Fig. 17. (*a*) Distribution of ε in the $Ri < 0.7$ range for the data in Figure 15. The mean value is approximately 10^{-7} m^2 s^{-3}. The vertical dashed line is the mean value. The leftmost dashed line represents the cumulative fraction while the other dashed line represents contribution to the mean. (*b*) Distribution of ε in the $Ri > 0.7$ range for the data in Figure 15.

to estimate the shear production of the turbulence. This estimate requires the surface layer to be a constant stress layer, an assumption for which we can offer no verification. The cruise-averaged value of $u_*^2\, dU/dz$ was 5 times larger than the cruise-averaged surface layer ε (Table 1). Therefore either u_*^2 was not representative of $\langle u'w' \rangle$ (that is, the surface layer was not a constant stress layer), or else the energy was carried off by other processes (for example, by internal waves radiated from the base of the mixed layer). Experimental studies [*Thorpe*, 1973; *Linden*, 1975; *Kantha*, 1979] indicate that internal waves generated in the mixed layer can effect a considerable energy flux out of the mixed layer. Calculations by *Bell* [1978] indicate that internal waves generated by such a mechanism can grow at the expense of the mean current shear. Unfortunately, we cannot estimate the internal wave energy flux with the available measurements.

8.2. *Thermocline*

The nature of the turbulence below the surface layer was markedly different from that in the surface layer. The turbulence below was highly intermittent, dominated by energetic bursts persisting for 2–3 hours and separated by several hours. The bursts began late at night and persisted many hours past sunrise. We suspect that the bursts were related to internal waves generated at the mixed layer base that radiate energy downward. The process would be similar to those observed in the laboratory studies and model calculations mentioned above. There is one clear example of breaking internal waves in towed thermistor chain measurements from our north-south transect in November 1984. Towed thermistor chain data show an energetic patch of breaking internal waves at night at 1.4°N [*Moum et al.*, 1986*a*]. Characteristic scales of the wave packet were 15 m in vertical displacement and 500 m in horizontal wavelength (N = 5–8 cph). RSVP profiles through the patch indicated a patch-averaged ε of 10^{-6} m^2 s^{-3}. There is also evidence for a diurnal cycle in internal wave activity from towed thermistor chain measurements and longer-term moored measurements (C. A. Paulson, personal communication, 1985). Unfortunately, the period of the internal waves is too short for them to be resolved by the RSVP casts, and the thermistor chain was not deployed on station (since the towed thermistor chain requires a mean flow for stability). Therefore we cannot verify our speculation that turbulent bursts below the surface layer were associated with breaking internal waves.

If the bursts are signatures of internal waves and each burst indicates a generation event, why does the equatorial ocean not maintain a constant level of internal wave activity? A possible explanation is that they break soon after generation, losing their energy locally to turbulent dissipation. The potential energy of the waves can be estimated from the local stratification and vertical displacement, ζ. In the energetic patch observed in the towed thermistor chain measurements, N was 0.01 s^{-1} and ζ was 15 m. The internal wave energy may be approximated by $N^2\zeta^2$ and the decay time for the internal wave field estimated as

$$\tau_d = N^2\zeta^2/\varepsilon \simeq 6 \text{ hours}$$

This estimate is approximately 100 times smaller than comparable estimates for open ocean thermoclines [*Lueck et al.*, 1983; *Moum and Osborn*, 1986]. Even though the equatorial internal waves are more energetic, they dissipate far more rapidly.

9. SUMMARY

For 12 days in late November 1984, meteorological conditions were relatively constant, with nearly cloudless skies and a wind stress that was never less than 0.05 N m^{-2} nor more than 0.15 N m^{-2} for more than a few hours. Large-scale currents and hydrographic fields were altered only by the passage of a pulse of thermocline deepening and by the near-surface meridional current associated with the 20-day wave. As a result, we were able to observe the response of the upper equatorial ocean to diurnal stimuli under fairly similar conditions. Our observations covered the weakly stratified surface layer, the thermocline above the EUC core, and the region of the core.

As was indicated in preliminary analyses, the main source of temporal variability was the diurnal cycle in surface buoyancy flux (there was no significant diurnal cycle in wind stress). In the daytime, when solar insolation dominated the buoyancy flux, turbulence was suppressed. At night, turbulence increased, especially in the thermocline below the weakly stratified surface layer and above the EUC core. In this region, turbulence appeared to propagate vertically at 5 m h^{-1} and sometimes persisted past daybreak. Mean values of ε were almost a factor of 10 smaller in the afternoon than the maximum values observed (at sunrise).

Three regimes were identified in which the behavior of ε was quite different:

1. In a weakly stratified region at the surface, active turbulence was present at all times. The thickness of this region, defined by the density step at its base, varied from less than 10 m during the day to more than 35 m on windy nights.

2. In the highly stratified region below the surface layer and above the EUC core, turbulence was highly intermittent. It tended to occur in bursts, at night or in the early morning. Ri was almost always low, but ε varied greatly.

3. In the region near the low-shear core of the EUC, the stratification was generally strong, Ri was almost always high, and ε was nearly always small.

Other sources of time variability in the mean field may have affected the turbulence:

1. The 4-day pulse of lowered thermocline depth decreased the vertical current shear and increased Ri above the EUC core; ε also decreased. However, at the same time the winds were exceptionally low, and meridional current speeds were unusually small, so the cause of lowered ε cannot be clearly identified.

2. The upper 50-m meridional current, which was weak in the first few days, became strong in the northward direction midway through the experiment. The vertical structure of this current identifies it almost certainly as the 20-day tropical wave. Changes in turbulence activity may have been related to this motion. (This wave had very little effect on the zonal current.)

In the surface layer and in that part of the thermocline above the EUC core, the heat was carried vertically primarily by turbulent diffusion (70%) rather than by irradiance. In the core the vertical heat flux was very small. The increased heat content in the upper layers was of the magnitude estimated for the heat advected from the south by the northward flowing meridional current associated with the 20-day wave.

The proper parameterization of ε or of turbulent transport coefficients is not obvious from our data. There is no sign of a functional dependence of ε on Ri. From our data, we found that the best description of the relationship of Ri and ε in the thermocline was as follows: for $Ri > 0.7$, ε had a mean value of 6.6×10^{-9} m^2 s^{-3} with a standard deviation of 1.4×10^{-8} m^2 s^{-3}, whereas for $Ri < 0.7$, the mean value of ε was 9.2×10^{-8} m^2 s^{-3} with a standard deviation of 1.7×10^{-7} m^2 s^{-3}.

Peters et al. [1988], using similar data, interpreted a rather different relationship. They also found a division between regimes, with a boundary at $Ri = 0.4$. At lower Ri they found a steep dependence of ε and turbulent transport coefficients on Ri (as $Ri^{-9.6}$ for K_h, for example). At higher Ri they found a gentle dependence. We cannot justify these forms on the basis of our data. Their data were obtained 20 km away, during the last 4.5 days of our observation period, with very similar but not exact methods.

Although the conditions necessary for mixing may well be indicated by a critical value of Ri, the magnitude of ε must depend on the direct forcing of the turbulence at the specific time and place of the mixing event. Therefore (and contrary to the opinion of *Peters et al.* [1988]), we feel that the quest for a simple Ri parameterization of turbulent mixing is doomed because it does not address the necessary physics of the problem.

Acknowledgments. We are grateful to the master and crew of the R/V *Wecoma* for their efforts in making the experimental effort successful, to Melora Park and Rick Baumann for computing support, to Ayal Anis for doing many of the statistical computations, and to David Halpern for allowing us to use some of the T44 mooring data. Numerous conversations with Teri Chereskin and Tom Dillon over the course of this work are acknowledged. We have enjoyed a fruitful working relationship with Hartmut Peters and Mike Gregg of the Applied Physics Laboratory, University of Washington. This work was conducted under grants OCE-8214639 and OCE-8608256 from the National Science Foundation.

REFERENCES

Bell, T. H., Radiation damping of inertial oscillations in the upper ocean, *J. Fluid Mech.*, *88*, 289–308, 1978.

Caldwell, D. R., Small-scale physics of the ocean, *Rev. Geophys., Phys.*, *21*, 1192–1205, 1983.

Caldwell, D. R., T. M. Dillon, and J. N. Moum, The rapid sampling vertical profiler: An evaluation, *J. Atmos. Oceanic Technol.*, *2*, 615–625, 1985.

Chereskin, T. K., J. N. Moum, P. J. Stabeno, D. R. Caldwell, C. A. Paulson, L. A. Regier, and D. Halpern, Fine-scale variability at 140°W in the equatorial Pacific, *J. Geophys. Res.*, *91*, 12,887–12,897, 1986.

Chereskin, T. K., D. Halpern, and L. A. Regier, Comparison of shipboard acoustic Doppler current profiler and moored current measurements in the equatorial Pacific, *J. Atmos. Oceanic Technol.*, *4*, 742–747, 1987.

Crawford, W. R., and T. R. Osborn, Energetics of the Atlantic equatorial undercurrent, *Deep Sea Res.*, GATE suppl. II, *26*, 309–324, 1979.

Crawford, W. R., and T. R. Osborn, Control of equatorial currents by turbulent dissipation, *Science*, *212*, 539–540, 1981.

Dillon, T. M., J. N. Moum, T. K. Chereskin, and D. R. Caldwell, On the zonal momentum balance at the equator, *J. Phys. Oceanogr.*, in press, 1988.

Dorrestein, R., On the vertical buoyancy flux below the sea surface as induced by atmospheric factors, *J. Phys. Oceanogr.*, *9*, 229–231, 1979.

Eriksen, C. C., Measurements and models of fine structure, internal gravity waves, and wave breaking in the deep ocean, *J. Geophys. Res.*, *83*, 2989–3009, 1978.

Gargett, A. E., T. R. Osborn, and P. W. Nasmyth, Local isotropy and the decay of turbulence in a stratified fluid, *J. Fluid Mech.*, *144*, 231–280, 1984.

Gregg, M. C., Temperature and salinity microstructure in the Pacific equatorial undercurrent, *J. Geophys. Res.*, *81*, 1180–1196, 1976.

Gregg, M. C., Diapycnal mixing in the thermocline, *J. Geophys. Res.*, *92*, 5249–5286, 1987.

Gregg, M. C., H. Peters, J. C. Wesson, N. S. Oakey, and T. J. Shay, Intensive measurements of turbulence and shear in the equatorial undercurrent, *Nature*, *318*, 140–144, 1985.

Head, M. J., The use of miniature four-electrode conductivity probes for high-resolution measurement of turbulent density or temperature variations in salt-stratified flows, Ph.D. thesis, 211 pp., Univ. of Calif., San Diego, 1983.

Hines, W. W., and D. C. Montgomery, *Probability and Statistics in Engineering and Management Science*, Ronald Press, New York, 1972.

Imawaki, S., P. P. Niiler, C. H. Gautier, D. Halpern, R. A. Knox, W. G. Large, D. S. Luther, J. C. McWilliams, J. N. Moum and C. A. Paulson, A new method for estimating the turbulent heat flux at the bottom of the daily mixed layer, *J. Geophys. Res.*, *93*, 14,005–14,012, 1988.

Kantha, L. H., On generation of internal waves by turbulence in the mixed layer, *Dyn. Atmos. Oceans*, *3*, 39–46, 1979.

Large, W. G., and S. Pond, Open ocean momentum flux measurements in moderate to strong winds, *J. Phys. Oceanogr.*, *11*, 324–336, 1981.

Linden, P. F., The deepening of a mixed layer in a stratified fluid, *J. Fluid Mech.*, *71*, 385–405, 1975.

Lueck, R. G., W. R. Crawford, and T. R. Osborn, Turbulent dissipation over the continental slope off Vancouver Island, *J. Phys. Oceanogr.*, *13*, 1809–1818, 1983.

McCreary, J. P., A linear stratified ocean model of the equatorial undercurrent, *Philos. Trans. R. Soc. London, Ser. A*, *298*, 603–635, 1981.

Miles, J. W., On the stability of heterogeneous shear flows, *J. Fluid Mech.*, *10*, 496–508, 1961.

Monin, A. S., and A. M. Yaglom, *Statistical Fluid Mechanics*, vol. 2, MIT Press, Cambridge, Mass., 1975.

Moum, J. N., and D. R. Caldwell, Local influences on shear-flow turbulence in the equatorial ocean, *Science*, *230*, 315–316, 1985.

Moum, J. N., and T. R. Osborn, Mixing in the main thermocline, *J. Phys. Oceanogr.*, *16*, 1250–1259, 1986.

Moum, J. N., D. R. Caldwell, C. A. Paulson, T. K. Chereskin, and L.

A. Regier, Does ocean turbulence peak at the equator?, *J. Phys. Oceanogr.*, *16*, 1991–1994, 1986*a*.

Moum, J N., T. R. Osborn, and W. R. Crawford, Pacific equatorial turbulence: Revisited, *J. Phys Oceanogr.*, *16*, 1516–1522, 1986*b*.

Oakey, N. S., Determination of the rate of dissipation of turbulent energy from simultaneous temperature and velocity shear microstructure measurements, *J. Phys. Oceanogr.*, *12*, 256–271, 1982.

Oakey, N. S., Statistics of mixing parameters in the upper ocean during JASIN Phase 2, *J. Phys. Oceanogr.*, *15*, 1662–1675, 1985.

Osborn, T. R., Estimates of the local rate of vertical diffusion from dissipation measurements, *J. Phys. Oceanogr.*, *10*, 83–89, 1980.

Osborn, T. R., and C. S. Cox, Oceanic fine structure, *Geophys Fluid Dyn.*, *3*, 321–345, 1972.

Osborn, T. R., and R. G. Lueck, Turbulence measurements with a submarine, *J. Phys. Oceanogr.*, *15*, 1502–1520, 1985*a*.

Osborn, T R., and R. G. Lueck, Turbulence measurements from a towed body, *J. Atmos. Oceanic Technol.*, *2*, 517–527, 1985*b*.

Park, M. M., J. N. Moum, D. R. Caldwell, P. J. Stabeno, J. L. Cantey, and S. D. Wilcox, Tropic Heat 1984 rapid sampling vertical profiler observations, *Ref. 85-21*, 395 pp., Coll. of Oceanogr., Oreg. State Univ., Corvallis, 1985.

Park, M. M., J. N. Moum, D. R. Caldwell, and M. D. Brown, Tropic Heat II 1987—Leg 1 rapid sampling vertical profiler observations, *Ref. 87-22*, 378 pp., Coll. of Oceanogr., Oreg. State Univ., Corvallis, 1987*a*.

Park, M. M., J. N. Moum, and D. R. Caldwell, Tropic Heat II 1987—Leg 2 rapid sampling vertical profiler observations, *Ref. 87-17*, 439 pp., Coll. of Oceanogr., Oreg. State Univ., Corvallis, 1987*b*.

Paulson, C A , and J. J. Simpson, Irradiance measurements in the upper ocean, *J. Phys. Oceanogr.*, *7*, 952–956, 1977.

Payne, R. E., Albedo of the sea surface, *J. Atmos. Sci.*, *29*, 959–970, 1972.

Peters, H., M. C. Gregg, and J. M. Toole, On the parameterization of equatorial turbulence, *J. Geophys. Res.*, *93*, 1199–1218, 1988.

Rohr, J., and C. Van Atta, Mixing efficiency in stably stratified growing turbulence, *J. Geophys Res.*, *92*, 5481–5488, 1987.

Shay, T J., and M. C. Gregg, Convectively driven turbulent mixing in the upper ocean, *J. Phys. Oceanogr.*, *16*, 1777–1798, 1986.

Thorpe, S. A., Turbulence in stably stratified fluids: A review of laboratory experiments, *Boundary Layer Meteorol.*, *5*, 95–119, 1973.

D. R. Caldwell, J. N. Moum, and C. A. Paulson, College of Oceanography, Oregon State University, Corvallis, OR 97331.

(Received February 16, 1988;
accepted April 25, 1988.)